Fingerprint and Universal Markovian Closure of Structured Bosonic Environments

Alexander Nüßeler,[1] Dario Tamascelli,[1,2] Andrea Smirne,[2,3] James Lim,[1]
Susana F. Huelga,[1] and Martin B. Plenio[1]

[1]*Institut für Theoretische Physik and IQST, Albert-Einstein-Allee 11, Universität Ulm, 89069 Ulm, Germany*
[2]*Dipartimento di Fisica "Aldo Pontremoli," Università degli Studi di Milano, Via Celoria 16, 20133 Milano, Italy*
[3]*Istituto Nazionale di Fisica Nucleare, Sezione di Milano, Via Celoria 16, 20133 Milano, Italy*

(Received 4 August 2022; accepted 7 September 2022; published 30 September 2022)

We exploit the properties of chain mapping transformations of bosonic environments to identify a finite collection of modes able to capture the characteristic features, or fingerprint, of the environment. Moreover we show that the countable infinity of residual bath modes can be replaced by a universal Markovian closure, namely, a small collection of damped modes undergoing a Lindblad-type dynamics whose parametrization is independent of the spectral density under consideration. We show that the Markovian closure provides a quadratic speedup with respect to standard chain mapping techniques and makes the memory requirement independent of the simulation time, while preserving all the information on the fingerprint modes. We illustrate the application of the Markovian closure to the computation of linear spectra but also to nonlinear spectral response, a relevant experimentally accessible many body coherence witness for which efficient numerically exact calculations in realistic environments are currently lacking.

DOI: 10.1103/PhysRevLett.129.140604

Much theoretical research in recent decades has focused on the study of open quantum systems (OQSs) interacting with structured non-Markovian environments [1–4]. Analytical results are hard to obtain except for very specific models, and numerical simulations are typically very challenging unless severe approximations are made. Despite these challenges, the interaction of an OQS with the surrounding environment is not only unavoidable in practice, but there are important instances where non-Markovianity may be instrumental for different manifestations of the presence of quantum coherence or quantum correlations to persist for significant timescales [5–9] or even in the thermodynamical limit [10–12].

For thermal bosonic environments, numerical methods developed for a general treatment of non-Markovian problems include, e.g., hierarchical equations of motion (HEOM) [13,14], quasiadiabatic path integrals (QUAPI) [15,16], nonequilibrium Green's function (NEGF) techniques [17,18], non-Markovian quantum state diffusion (NMQSD) and similar stochastic methods [19–21] and the time-evolving density operator with orthogonal polynomials algorithm (TEDOPA) [5,22–27]. Recently, powerful hybrid methods have been developed including the time-evolving matrix product operators (TEMPO) [28], merging path integral and tensor network methods, the dissipation-assisted matrix product factorization (DAMPF) [29,30], combining tensor networks and local Markovian dissipators and methodologies that utilize tensor networks in combination with quantum state diffusion [31]. In this work we will develop an exact hybrid scheme that combines the intuition behind strategies aimed at redefining the system-environment boundary by means, for instance, of introducing a reaction coordinate [32] or utilizing surrogate oscillator modes [33] with chain mapping transformations as those implemented by TEDOPA [22].

TEDOPA is a certifiable and numerically exact method to efficiently treat OQS dynamics. It first maps the continuum of bath modes unitarily onto a one-dimensional chain of harmonic oscillators, and then it exploits time-dependent density matrix renormalization group (TDMRG) [34] to efficiently simulate the dynamics of the resulting configuration. Besides providing an optimal discretization of the bath [35], TEDOPA treats the OQS and the bath degrees of freedom on the same footing, thus leaving the possibility of inspecting the evolution of both. Moreover, unlike some of the methods mentioned in the previous paragraph, TEDOPA is not restricted to thermal or Gaussian initial states of the environment. However, despite

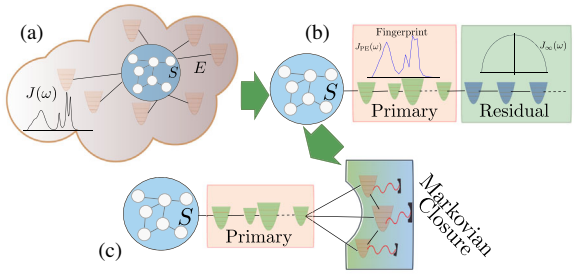

FIG. 1. Schematics of our procedure: (a) The system (S) interacting with a bosonic environment (E), as described by Eqs. (1)–(4). (b) After the chain-mapping, the system interacts with the primary environment, which interacts in turn with the residual environment. (c) The residual environment is replaced by a finite set of interacting damped modes, i.e., the Markovian closure.

its usefulness TEDOPA, as all methods mentioned earlier, remains computationally intensive. In order to address more challenging questions, such as the determination of multidimensional spectra [36,37], further efficiency gains are required.

We will exploit the properties of the TEDOPA mapping to show that the main features, or fingerprint, of the environment are captured by a primary bath comprising a finite, and typically small, number of modes directly interacting with the OQS. Moreover, we show that the remaining environmental modes form a universal residual bath and that such a residual bath can be replaced by a finite number of damped harmonic modes undergoing a Lindblad-type dynamics (See Fig. 1). We provide an explicit construction of this universal Markovian closure and illustrate that the ensuing reduction of the computational resources renders the calculation of 2D nonlinear electronic spectra [36,37] accessible to this method.

TEDOPA mapping.—We consider a system interacting with a bosonic environment. The complete Hamiltonian reads

$$H = H_S + H_E + H_I \tag{1}$$

$$H_E = \int d\omega\, \omega a_\omega^\dagger a_\omega \tag{2}$$

$$H_I = \int d\omega\, h(\omega)(A_S^\dagger a_\omega + A_S a_\omega^\dagger), \tag{3}$$

($\hbar = 1$) where H_S is the (arbitrary) free system Hamiltonian, H_E describes the free evolution of the bosonic environmental degrees of freedom, and H_I is the bilinear system-environment interaction Hamiltonian [38]. Moreover we assume that $h(\omega)$ has finite support $[\omega_{\min}, \omega_{\max}]$, $\omega_{\min} < \omega_{\max}$, and introduce the spectral density

$$J(\omega) = \pi h^2(\omega). \tag{4}$$

As shown in [5,22,39] the Hamiltonian (1) can be unitarily mapped to an equivalent one describing a countably infinite set of modes with operators $b_n^{(\dagger)}$ satisfying the bosonic commutation relations $[b_n, b_m^\dagger] = \delta_{nm}$ yielding

$$\begin{aligned} H^C &= H_S + H_I^C + H_E^C, \\ H_I^C &= \kappa_0(A_S^\dagger b_1 + A_S b_1^\dagger), \\ H_E^C &= \sum_{n=1}^{\infty} \omega_n b_n^\dagger b_n + \kappa_n(b_{n+1}^\dagger b_n + b_n^\dagger b_{n+1}), \end{aligned} \tag{5}$$

where the coefficients ω_n and κ_n, are determined either analytically [22] or numerically [40,41].

For the following, the joint initial state of system and environment is assumed to factorize, i.e., $\varrho_{SE}(0) = \varrho_S(0) \otimes \varrho_E(0)$, with $\varrho_E(0)$ a thermal state. Following [26], it is possible to replace $\varrho_E(0)$ with the factorized pure vacuum state when performing at the same time a suitable transformation of the spectral density.

Bath fingerprint and universal closure.—As shown in [22,39], the asymptotic values of the chain mode frequencies ω_n and coupling constants κ_n are

$$\begin{aligned} \omega_n &\underset{n\to\infty}{\longrightarrow} \frac{\omega_{\min} + \omega_{\max}}{2} \overset{\text{def}}{=} \Omega, \\ \kappa_n &\underset{n\to\infty}{\longrightarrow} \frac{\omega_{\max} - \omega_{\min}}{4} \overset{\text{def}}{=} K. \end{aligned} \tag{6}$$

Given the spectral density $J(\omega)$, for any $M > 0$ we define the Hamiltonian of the residual bath as

$$H_R = \Omega \sum_{m=M+1}^{\infty} b_m^\dagger b_m + K \sum_{m=M+1}^{\infty} (b_{m+1}^\dagger b_m + b_m^\dagger b_{m+1}), \tag{7}$$

where H_R is obtained from H_E^C by disregarding the first M modes and replacing the chain coefficients ω_m/κ_m with their asymptotic values. For a given value of M the original system-environment Hamiltonian (5) is approximated by

$$\tilde{H} = H_S + H_I^C + H_{\mathrm{PE}} + \kappa_M(b_M^\dagger b_{M+1} + \mathrm{H.c.}) + H_R, \tag{8}$$

$$H_{\mathrm{PE}} = \sum_{n=1}^{M} \omega_n b_n^\dagger b_n + \sum_{n=1}^{M-1} \kappa_n(b_n^\dagger b_{n+1} + b_n b_{n+1}^\dagger). \tag{9}$$

Of course, equality $\tilde{H} = H^C$ holds only in the $M \to \infty$ limit: for finite values of M only the chain coefficients associated with the first M chain sites are exact, while the remaining ones are only approximated. Such an approximation is, however, under full control: the exact coefficients are known and the effects of small variations of the spectral density on the system dynamics can be bounded analytically [42]. In what follows we denote with $M(\varepsilon)$ the smallest M such that $|(\omega_m - \Omega)/\Omega|$, $|(\kappa_m - K)/K| < \varepsilon$, $\forall\ m \geq M$; we moreover chose $\varepsilon = 10^{-3}$ and denote this case as ε converged, but other choices can be used.

The exact part of the chain, comprising the first M modes, plays the role of *primary environment* (PE), capturing the specific features, or *fingerprint*, of the spectral density (see Fig. 1). This is exemplified in Fig. 2 where we consider an environmental spectral density $J(\omega) = J_{\mathrm{AR}}(\omega) + \sum_{k=1}^{3} J_{L,k}(\omega)$ of a photosynthetic pigment-protein complex, water-soluble chlorophyll-binding protein (WSCP) from cauliflower [43]. Here $J_{\mathrm{AR}}(\omega)$ is a broad phonon spectrum originating from protein motions [43] while three narrow Lorentzian peaks $J_{L,k}(\omega)$ describe intrapigment vibrational modes [44] with vibrational frequencies $(\Omega_1, \Omega_2, \Omega_3) = (181, 221, 240)$ cm^{-1} and an

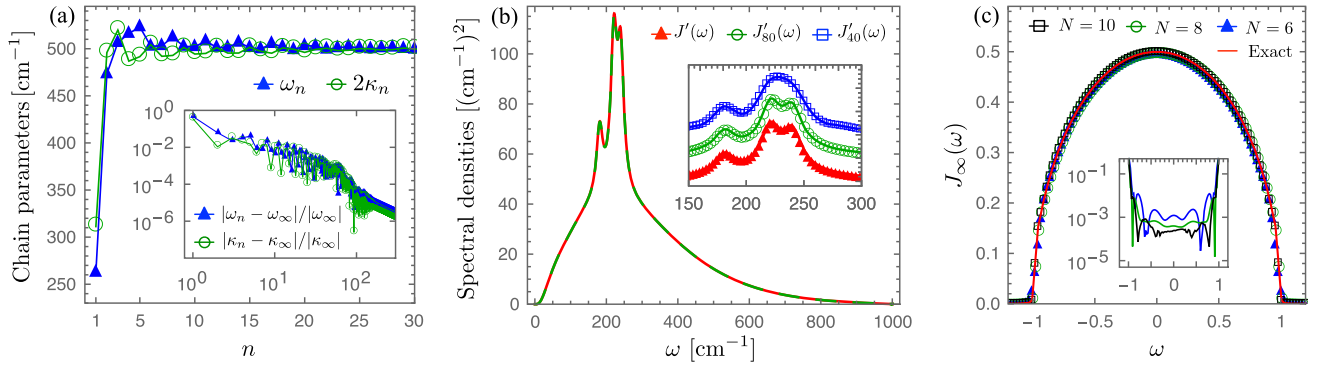

FIG. 2. Coefficients, fingerprint, and closure: (a) The TEDOPA chain oscillator frequencies ω_n (blue triangles) and couplings κ_n (green circles) obtained for the WSCP spectral density $J(\omega)$ described in the main text. In the inset the relative errors between the exact and asymptotic coefficients. (b) The effective spectral density $J'(\omega)$ of the TEDOPA chain truncated after 400 sites (red line) and the effective spectral density $J'_M(\omega)$ with the asymptotic values Ω/K replacing the exact coefficients ω_n/κ_n for $n > M = 80$ (dashed green line). In the inset, the effective spectral densities $J'(\omega)$, $J'_{80}(\omega)$, $J'_{40}(\omega)$ (vertically shifted for improved visibility). (c) The residual spectral density (10) for $[\omega_{\min}, \omega_{\max}] = [-1, 1]$ and the approximation provided by the TSO with $N = 6, 8, 10$ auxiliary modes; inset: the relative error $|J_\infty(\omega) - J_N^{\mathrm{TSO}}(\omega)|/J_\infty(\omega)$ for $\omega \in [-1, 1]$.

energy damping rate on the picosecond timescale (see the Supplemental Material (SM) [45] for more details). The domain $[\omega_{\min}, \omega_{\max}] = [0, 1000]$ cm^{-1} of $J(\omega)$ is chosen such that the discarded weight $W_d(\omega_{\max}) := \int_{\omega_{\max}}^{\infty} d\omega' J(\omega')/\int_0^{\infty} d\omega' J(\omega') < 10^{-3}$. As Fig. 2(a) shows, the chain coefficients ω_n, κ_n are $\varepsilon = 10^{-3}$-converged for $M \approx 10^2$. In order to better illustrate the meaning of the fingerprinting modes, it is appropriate to truncate the TEDOPA chain after a finite number of sites, thus comparing discrete spectral densities to discrete spectral densities. In Fig. 2(b), the effective spectral density $J'(\omega)$ corresponding to a chain truncated after 400 sites is shown in red. Figure 2(b) also shows the effective spectral density $J'_M(\omega)$ obtained by replacing the exact coefficients ω_n/κ_n of the truncated TEDOPA chain with their asymptotic values Ω/K for $n > M$. It is clear that $J'_M(\omega)$ is in excellent agreement with the exact $J'(\omega)$ for $M \gtrsim 80$: the three narrow Lorentzian peaks of the WSCP spectral density in the region $\omega \in [150, 300]$ cm^{-1} are well resolved for $M = 80$, while for $M = 40$ the fine structure is lost, as shown in the inset of Fig. 2(b) (see also the SM [45]). The fingerprint of the WSCP spectral density is therefore provided by a PE consisting of a finite number M of sites; a suitable value of M can be determined by means of the ε-convergence criterion, which in turn determines the number of sites after which the exact semi-infinite chain, comprising the modes with $n > M$, is practically indistinguishable from an approximating *residual environment* governed by H_R [see Eq. (7)].

Markovian closure.—The spectral density of the residual environment reads [22,39]

$$J_\infty(\omega) = K^2 \frac{\sqrt{(\omega - \omega_{\min})(\omega_{\max} - \omega)}}{2}, \tag{10}$$

also known as the Winger semicircle [59,60]. Since $J_\infty(\omega)$ does not depend on the specific spectral density that we started with, but only on $\omega_{\min/\max}$, the residual environment is universal. Because of the translational invariance of the residual environment, an excitation entering the semi-infinite homogeneous part of the chain propagates ballistically away from the PE [27] at a speed proportional to K. On the one hand, this observation makes it clear that to avoid finite-size effects on the dynamics of the system, or of the PE, the truncation of the (semi-infinite) chain, which is required to enable simulations, must be suitably chosen: for a given simulation time T the length of truncated chain must be proportional to KT. Longtime simulations can therefore become computationally highly demanding, since a very large number of chain oscillators must be considered. On the other hand, the same ballistic propagation provides a suggestive picture of the irreversibility of the interaction of the extended system with the residual environment, with the latter "absorbing" all the excitations coming from the primary environment. Our findings show that such an absorption mechanism can be realized by means of a finite environment made up of a small collection of harmonic oscillators governed by the nearest-neighbor coupling Hamiltonian

$$H_{\mathrm{aux}} := \sum_{n=1}^{N} \Omega_n d_n^\dagger d_n + \sum_{n=1}^{N-1} g_n (d_{n+1}^\dagger d_n + d_n^\dagger d_{n+1}) \tag{11}$$

and subject to the local Lindblad dissipator

$$\mathcal{D}(\varrho) := \sum_{n=1}^{N} \Gamma_n \left(d_n \varrho d_n^\dagger - \frac{1}{2} \{ d_n^\dagger d_n, \varrho \} \right), \tag{12}$$

where ϱ is a statistical operator living on the Hilbert space of the surrogate oscillators providing a Markovian closure (MC) of the chain (see Fig. 1). For given N, the coefficients Γ_n, Ω_n, g_n are determined by means of the Transformation to Surrogate Oscillators (TSOs) procedure [33,61]. It is important to stress here that the universality of the residual spectral density J_∞ implies that the derivation of the TSO coefficients must be done only once. Figure 2(c) shows the spectral density of the auxiliary system provided by the TSOs for the choices $N = 6$, 8, 10, and allows one to appreciate the accuracy of the approximation of J_∞. Full detail on the TSO derivation and the values of the TSO parameters for different closure sizes are provided in the SM [45]. The use of MC is most effective when longtime dynamics is considered. In this case, in fact, standard TEDOPA would require the use of very long chains as not to produce finite-size effects affecting the system and the extended system, comprising the system and the PE, dynamics. In what follows we describe a relevant application of the MC.

Application: longtime system dynamics.—To demonstrate that our construction allows for numerically exact longtime simulations, we investigate optical responses of a model molecular complex, WSCP, an aggregate for which a comprehensive spectral charaterization is available [43]. The dimeric system consists of two interacting pigments, with each pigment coupled to a local phonon environment characterized by $J(\omega)$. Motivated by the actual parameters of WSCP, we model each pigment as a two-level system with an identical energy gap between electronic ground and excited states ($\sim$15 198 cm^{-1}) and consider an electronic coupling 69 cm^{-1} between pigments (see the SM [45]). As to make most of the details of the spectra clearly visible, we consider a phonon bath at zero temperature and parallel transition dipoles of pigments. In this setting the relevant state space is spanned by a low-energy optically dark electronic eigenstate (or exciton) $|E_d\rangle$, and a bright high-energy exciton state $|E_b\rangle$, which dominates the optical responses. As shown in Fig. 3(a), the (numerically exact) absorption spectrum computed by the MC cannot be reproduced by a line shape theory based on second order cumulant expansion [62–64], which has been widely used to simulate optical responses of photosynthetic systems. The absorption spectrum can be better reproduced by a reduced vibronic model where the three narrow peaks $J_{L,k}(\omega)$ in the spectral density are included in the system Hamiltonian in addition to electronic states, and the remaining broad environmental spectrum $J_{\mathrm{AR}}(\omega)$ is considered a source of Markovian noise [65,66]. However, the low-energy part of the absorption spectrum cannot be reproduced. The numerically exact absorption spectrum can be well reproduced only when multiple narrow Lorentzian functions are fitted to the spectral density $J_{\mathrm{AR}}(\omega)$ and each Lorentzian is considered a damped harmonic oscillator coupled to electronic states [61].

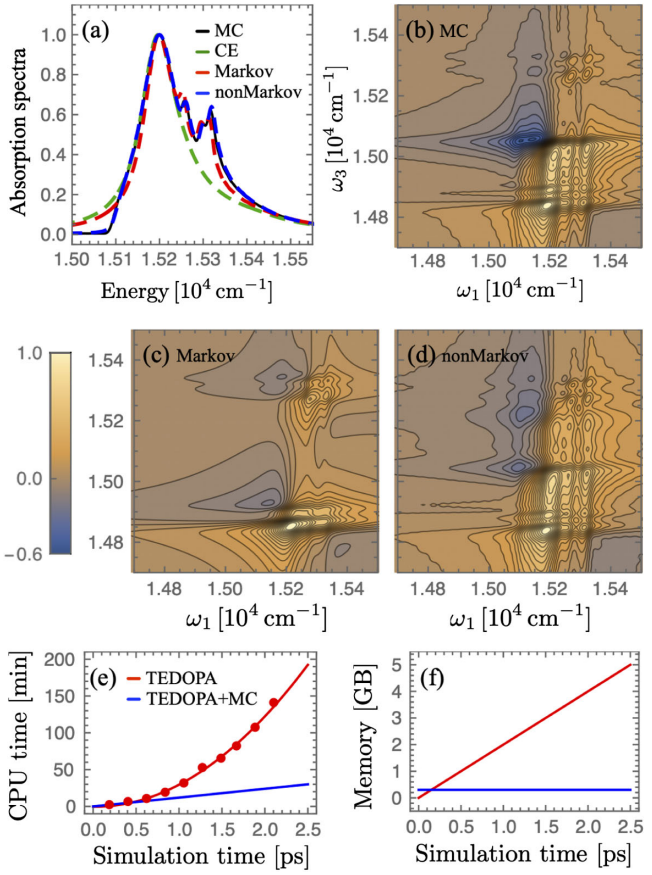

FIG. 3. Linear and 2DES optical spectra of WSCP, computational cost: (a) Absorption spectra computed by TEDOPA with Markovian closure (MC), cumulant expansion (CE), reduced vibronic models with Markovian and non-Markovian effects of a broad environmental spectrum $J_{\mathrm{AR}}(\omega)$. 2D electronic spectra at $t_2 = 500$ fs computed by (b) MC, and reduced vibronic models with (c) Markovian and (d) non-Markovian effects of the broad noise spectrum. The time (e) and memory scaling (f) as functions of the simulation time $t_{\max}$.

Such a non-Markovian treatment of the broad environmental spectrum $J_{\mathrm{AR}}(\omega)$ enables one to successfully reproduce a numerically exact absorption line shape, as shown in Fig. 3(a). For more details of the reduced models and the origin of absorption peaks, see the SM [45].

The non-Markovian treatment of the broad environmental spectrum becomes more important when longtime system dynamics is considered. As an example, we consider two-dimensional electronic spectroscopy (2DES) [36,37], which is a time-resolved optical technique for measuring electronic and vibrational dynamics [65,67–70]. In 2DES, a sample is perturbed by three laser pulses with controlled time delays, enabling one to investigate molecular dynamics as a function of excitation ω_1 and detection energies ω_3 for each time delay t_2 between the second and the third pulse. Figure 3(b) shows a numerically exact stimulated emission component of rephasing 2D spectra at a waiting time $t_2 = 500$ fs (see the SM [45]), where

multiple 2D peaks are present for $\omega_3 < \omega_1$. These results cannot be reproduced by a reduced vibronic model when the broad phonon spectrum $J_{\mathrm{AR}}(\omega)$ is considered a source of the Markovian noise, as shown in Fig. 3(c). In order to better reproduce the numerically exact nonlinear optical responses, it is necessary to include the non-Markovian effects of the broad noise spectrum in the reduced model [see Fig. 3(d)]. These non-Markovian features in 2DES originate from multiphonon transitions where initial bright exciton state $|E_b, 0\rangle$ is vibronically mixed with lower-energy dark exciton states $|E_d, 1_j\rangle$ while creating a single vibrational excitation in the jth mode, and then goes back to the bright exciton states $|E_b, 1_j, 1_k\rangle$ while creating an additional vibrational excitation in the kth mode. As the single-phonon transitions result in optically dark states $|E_d, 1_k\rangle$, the multiphonon transitions can dominate 2D line shape when the system has enough time to evolve from the initial vibrational ground state $|E_b, 0\rangle$ to the final doubly excited vibrational states $|E_b, 1_j, 1_k\rangle$, as is the case of the long waiting time $t_2 = 500$ fs considered here. These results could be most relevant in the interpretation of optical responses of charge-separating systems, such as reaction centers in photosynthetic systems [68,69] and organic solar cells [71], where light-absorbing bright excitons relax to optically dark charge-transfer states where electrons and holes are spatially separated while creating vibrational excitations.

Performance.—In order to allow for a comparison with the results obtained by a standard TEDOPA implementation, we limited our investigation to waiting time $t_2 = 500$ fs, resulting in an overall simulation time of up to 2.5 ps. For such evolution times, converged TEDOPA simulations required about $N = 240$ chain sites to avoid any finite size effects, whereas with the MC only $M + 6 = 86$ sites were needed for $\varepsilon = 10^{-3}$ convergence of the chain coefficients. This translates into a significant reduction of the computational cost: the computation time is reduced from ≈190 min to ≈30 min (using 12 Intel Xeon Cascade Lake cores) while the memory consumption is reduced from ≈5 GB to ≈300 MB. Most importantly, the MC allows for a quadratic speedup of TEDOPA simulations for given simulated physical time. As a matter of fact, for standard TEDOPA the length of the chain increases linearly with the simulation time t_{max}, resulting in a CPU time cost $O(t_{\mathrm{max}}^2)$, whereas for the MC this cost is reduced to $O(t_{\mathrm{max}})$. For the same reason, the memory required by TEDOPA simulations scales linearly with t_{max} while the MC the memory requirement is constant, as shown in Figs. 3(e) and 3(f).

Conclusion and outlook.—Besides providing a clear computational advantage when longtime evolution is considered, the MC preserves the possibility offered by TEDOPA to treat the system and the (primary) environment on the same footing. The information on the relevant environmental degrees of freedom, the fingerprint, is therefore fully available for inspection. In this sense, the MC is complementary to standard TEDOPA and provides us with a most powerful tool for the study of unitary equilibration processes in fundamental systems such as the single-impurity Anderson model [60,72–74] and in the context of quantum thermodynamics [75,76]. Moreover, we expect the MC to be able to significantly reduce the computational overhead in situations characterized by long-range correlations between different environments, as in 1D transport models [25,77], and electron scattering problems where the populations of the electron wave packets propagating through semi-infinite electrodes after scattering events are evaluated [78]. The definition of the environmental fingerprint can also be exploited in other simulation techniques, such as HEOM, to simplify the fitting procedure [66,76]. In future work we will exploit the MC for the determination of higher order multiphonon transitions and the computation of the nonlinear spectral response of aggregates of biological relevance as well as for the study of energy and charge transfer in general many body systems and specifically light harvesting aggregates of both natural and artificial nature.

This work was supported by the DFG via QuantERA project ExtraQt and the ERC Synergy grant HyperQ, and support by the state of Baden-Württemberg through bwHPC and the German Research Foundation (DFG) through Grant No INST 40/575-1 FUGG (JUSTUS 2 cluster).

[1] A. Rivas, S. F. Huelga, and M. B. Plenio, Rep. Prog. Phys. **77**, 094001 (2014).
[2] H.-P. Breuer, E.-M. Laine, J. Piilo, and B. Vacchini, Rev. Mod. Phys. **88**, 021002 (2016).
[3] I. de Vega and D. Alonso, Rev. Mod. Phys. **89**, 015001 (2017).
[4] L. Li, M. J. Hall, and H. M. Wiseman, Phys. Rep. **759**, 1 (2018).
[5] J. Prior, A. W. Chin, S. F. Huelga, and M. B. Plenio, Phys. Rev. Lett. **105**, 050404 (2010).
[6] N. Christensson, H. F. Kauffmann, T. Pullerits, and T. Mancal, J. Phys. Chem. B **116**, 7449 (2012).
[7] V. Tiwari, W. K. Peters, and D. M. Jonas, Proc. Natl. Acad. Sci. U.S.A. **110**, 1203 (2013).
[8] A. Chin, J. Prior, R. Rosenbach, F. Caycedo-Soler, S. F. Huelga, and M. B. Plenio, Nat. Phys. **9**, 113 (2013).
[9] S. Tomasi, D. M. Rouse, E. M. Gauger, B. W. Lovett, and I. Kassal, J. Phys. Chem. Lett. **12**, 6143 (2021).
[10] S. F. Huelga, A. Rivas, and M. B. Plenio, Phys. Rev. Lett. **108**, 160402 (2012).
[11] D. Heineken, K. Beyer, K. Luoma, and W. T. Strunz, Phys. Rev. A **104**, 052426 (2021).
[12] A. Ask and G. Johansson, Phys. Rev. Lett. **128**, 083603 (2022).
[13] Y. Tanimura and R. Kubo, J. Phys. Soc. Jpn. **58**, 101 (1989).
[14] Y. Tanimura, Phys. Rev. A **41**, 6676 (1990).
[15] N. Makri, Chem. Phys. Lett. **193**, 435 (1992).

[16] M. Topaler and N. Makri, Chem. Phys. Lett. **210**, 285 (1993).
[17] J. Rammer and A. Schmid, Phys. Rev. B **34**, 1352(R) (1986).
[18] P. Danielewicz, Ann. Phys. (N.Y.) **152**, 239 (1984).
[19] L. Diósi and W. T. Strunz, Phys. Lett. A **235**, 569 (1997).
[20] L. Diósi and L. Ferialdi, Phys. Rev. Lett. **113**, 200403 (2014).
[21] J. Piilo, S. Maniscalco, K. Härkönen, and K.-A. Suominen, Phys. Rev. Lett. **100**, 180402 (2008).
[22] A. W. Chin, A. Rivas, S. F. Huelga, and M. B. Plenio, J. Math. Phys. (N.Y.) **51**, 092109 (2010).
[23] D. Tamascelli, R. Rosenbach, and M. B. Plenio, Phys. Rev. E **91**, 063306 (2015).
[24] M. P. Woods, M. Cramer, and M. B. Plenio, Phys. Rev. Lett. **115**, 130401 (2015).
[25] L. Kohn, F. Tschirsich, M. Keck, M. B. Plenio, D. Tamascelli, and S. Montangero, Phys. Rev. E **97**, 013301 (2018).
[26] D. Tamascelli, A. Smirne, J. Lim, S. F. Huelga, and M. B. Plenio, Phys. Rev. Lett. **123**, 090402 (2019).
[27] D. Tamascelli, Entropy **22**, 1320 (2020).
[28] A. Strathearn, P. Kirton, D. Kilda, J. Keeling, and B. W. Lovett, Nat. Commun. **9**, 3322 (2018).
[29] A. D. Somoza, O. Marty, J. Lim, S. F. Huelga, and M. B. Plenio, Phys. Rev. Lett. **123**, 100502 (2019).
[30] A. D. Somoza, N. Lorenzoni, J. Lim, S. F. Huelga, and M. B. Plenio, arXiv:2205.06623.
[31] S. Flannigan, F. Damanet, and A. J. Daley, Phys. Rev. Lett. **128**, 063601 (2022).
[32] P. Strasberg, G. Schaller, N. Lambert, and T. Brandes, New J. Phys. **18**, 073007 (2016).
[33] F. Mascherpa, A. Smirne, A. D. Somoza, P. Fernández-Acebal, S. Donadi, D. Tamascelli, S. F. Huelga, and M. B. Plenio, Phys. Rev. A **101**, 052108 (2020).
[34] U. Schollwöck, Ann. Phys. (Amsterdam) **326**, 96 (2011).
[35] I. de Vega, U. Schollwöck, and F. A. Wolf, Phys. Rev. B **92**, 155126 (2015).
[36] D. M. Jonas, Annu. Rev. Phys. Chem. **54**, 425 (2003).
[37] T. Brixner, T. Mancal, I. V. Stiopkin, and G. R. Fleming, J. Chem. Phys. **121**, 4221 (2004).
[38] A. J. Leggett, S. Chakravarty, A. T. Dorsey, M. P. A. Fisher, A. Garg, and W. Zwerger, Rev. Mod. Phys. **59**, 1 (1987).
[39] M. P. Woods, R. Groux, A. W. Chin, S. F. Huelga, and M. B. Plenio, J. Math. Phys. (N.Y.) **55**, 032101 (2014).
[40] W. Gautschi, ACM Trans. Math. Softw. **20**, 21 (1994).
[41] W. Gautschi, *Orthogonal Polynomials Computation and Approximation* (Oxford Science Publications, Oxford, 2004).
[42] F. Mascherpa, A. Smirne, S. F. Huelga, and M. B. Plenio, Phys. Rev. Lett. **118**, 100401 (2017).
[43] T.-C. Dinh and T. Renger, J. Chem. Phys. **142**, 034104 (2015).
[44] J. Pieper, M. Rätsep, I. Trostmann, H. Paulsen, G. Renger, and A. Freiberg, J. Phys. Chem. B **115**, 4042 (2011).
[45] See Supplemental Material at http://link.aps.org/supplemental/10.1103/PhysRevLett.129.140604 for additional information on the WSCP spectral density, on the derivation of the Markovian closure coefficients, on the TDVP simulations parameters, and for an introduction to linear and 2-dimensional electronic spectroscopy, together with a discussion the findings allowed by the proposed Markovian closure procedure, , which includes Refs. [46–58].
[46] H. Satoh, A. Uchida, K. Nakayama, and M. Okada, Plant Cell Physiol. **42**, 906 (2001).
[47] J. Lim, M. Tame, K. H. Yee, J.-S. Lee, and J. Lee, New J. Phys. **16**, 018001 (2014).
[48] S. Mukamel, *Principles of Nonlinear Optical Spectroscopy* (Oxford University Press, Oxford, 1995).
[49] V. May and O. Kühn, *Charge and Energy Transfer Dynamics in Molecular Systems: A Theoretical Introduction* (Wiley-VCH, Berlin, 2000).
[50] H.-P. Breuer and F. Petruccione, *The Theroy of Open Quantum Systems* (Oxford University Press, Oxford, 2002).
[51] T. Renger, M. E. Madjet, A. Knorr, and F. Müh, Journal of plant physiology **168**, 1497 (2011).
[52] F. Müh and T. Renger, Biophys. Acta **1817**, 1446 (2012).
[53] G. Beylkin and L. Monzón, Appl. Comput. Harmon. Anal. **19**, 17 (2005).
[54] B. M. Garraway, Phys. Rev. A **55**, 2290 (1997).
[55] V. May and O. Kühn, *Charge and Energy Transfer Dynamics in Molecular Systems* (John Wiley & Sons, New York, 2011).
[56] K. Hornberger, Introduction to decoherence theory, in *Entanglement and Decoherence: Foundations and Modern Trends*, edited by A. Buchleitner, C. Viviescas, and M. Tiersch (Springer Berlin Heidelberg, Berlin, Heidelberg, 2009), pp. 221–276.
[57] C. Lubich, I. V. Oseledets, and B. Vandereycken, SIAM J. Numer. Anal. **53**, 917 (2015).
[58] J. Haegeman, C. Lubich, I. Oseledets, B. Vandereycken, and F. Verstraete, Phys. Rev. B **94**, 165116 (2016).
[59] L. Arnold, Probab. Theory Relat. Fields **19**, 191 (1971).
[60] L. Kohn and G. E. Santoro, Phys. Rev. B **104**, 014303 (2021).
[61] D. Tamascelli, A. Smirne, S. F. Huelga, and M. B. Plenio, Phys. Rev. Lett. **120**, 030402 (2018).
[62] V. I. Novoderezhkin, M. A. Palacios, H. van Amerongen, and R. van Grondelle, J. Phys. Chem. B **108**, 10363 (2004).
[63] J. Adolphs and T. Renger, Biophys. J. **91**, 2778 (2006).
[64] D. Abramavicius and S. Mukamel, J. Chem. Phys. **133**, 184501 (2010).
[65] J. Lim, D. Paleček, F. Caycedo-Soler, C. N. Lincoln, J. Prior, H. von Berlepsch, S. F. Huelga, M. B. Plenio, D. Zigmantas, and J. Hauer, Nat. Commun. **6**, 7755 (2015).
[66] F. Caycedo-Soler, A. Mattioni, J. Lim, T. Renger, S. Huelga, and M. Plenio, Nat. Commun. **13**, 2912 (2022).
[67] M. B. Plenio, J. Almeida, and S. F. Huelga, J. Chem. Phys. **139**, 235102 (2013).
[68] E. Romero, R. Augulis, V. I. Novoderezhkin, M. Ferretti, J. Thieme, D. Zigmantas, and R. van Grondelle, Nat. Phys. **10**, 676 (2014).
[69] F. D. Fuller, J. Pan, A. Gelzinis, V. Butkus, S. S. Senlik, D. E. Wilcox, C. F. Yocum, L. Valkunas, D. Abramavicius, and J. P. Ogilvie, Nat. Chem. **6**, 706 (2014).
[70] J. Lim, C. M. Bösen, A. D. Somoza, C. P. Koch, M. B. Plenio, and S. F. Huelga, Phys. Rev. Lett. **123**, 233201 (2019).
[71] A. De Sio, F. Troiani, M. Maiuri, J. Réhault, E. Sommer, J. Lim, S. F. Huelga, M. B. Plenio, C. A. Rozzi, G. Cerullo, E. Molinari, and C. Lienau, Nat. Commun. **7**, 13742 (2016).

[72] P. W. Anderson, Phys. Rev. **124**, 41 (1961).
[73] F. Schwarz, I. Weymann, J. von Delft, and A. Weichselbaum, Phys. Rev. Lett. **121**, 137702 (2018).
[74] A. Nüßeler, I. Dhand, S. F. Huelga, and M. B. Plenio, Phys. Rev. B **101**, 155134 (2020).
[75] S.-J. Ran, B. Xi, C. Peng, G. Su, and M. Lewenstein, Phys. Rev. B **99**, 205132 (2019).
[76] S. Sakamoto and Y. Tanimura, J. Chem. Phys. **153**, 234107 (2020).
[77] I. de Vega and M.-C. Bañuls, Phys. Rev. A **92**, 052116 (2015).
[78] C. Vittmann, R. K. Kessing, J. Lim, S. F. Huelga, and M. B. Plenio, J. Phys. Chem. Lett. **13**, 1791 (2022).